

DOI: 10.1002/zaac.202200097

Free-Standing Few-Layer Tellurene Nanosheets: Simple Solution-Phase Synthesis and Electronic Structure

Animesh Bhui,^[a] Subhajit Roychowdhury,^[a] Arpita Sen,^[b] Umesh V. Waghmare,^[b] and Kanishka Biswas^{*[a, c]}

Dedicated to Prof. Mercuri G. Kanatzidis on the occasion of his 65th birthday.

Mechanical stirring of bulk Te in N-methyl-2-pyrrolidone (NMP) solution at room temperature resulted in the formation of free-standing few-layer (~1.2–2.8 nm) crystalline ultrathin nanosheets of tellurene with a large lateral thickness (~1–1.6 μm) as confirmed by atomic force microscopy (AFM). High-resolution transmission electron microscopy (HRTEM) confirms the pres-

ence of α - and β -phases of tellurene. First-principle density functional theoretical (DFT) based electronic structure calculations demonstrate the indirect band gap of bi-layer β -tellurene. The band gap decreases with increasing number of layers in the tellurene nanosheet.

Immense efforts have been devoted to discover new 2D materials and studying their physico-chemical properties, since the breakthrough discovery of graphene.^[1–3] Recently, 2D tellurium (Te) nanostructures are emerging as potential candidates for optoelectronics,^[4] energy-conversions,^[5–8] and chemical sensor^[9] applications due to its striking features, like tunable thickness-dependent band gap,^[10,11] excellent on-state current density,^[12] and decent carrier mobility with superior air-stability.^[12–14] Elemental Te has a bulk trigonal (t) crystal lattice with a space group $P3_121$ and an anisotropic helical structure in which helical chains of Te remain stacked via weak van der Waals forces, spiraling around the axis parallel to the c -axis.^[15,16] Due to the inherent structural anisotropy, earlier reported synthesis approaches predominantly produced several one-dimensional (1D)-nanostructures e.g., nanorods, nanowires, nanobelts, and nanotubes, etc.^[17,18] Very recently the work on morphology switching from 1D to 2D started with the motivation from theoretical predictions of several quasi-stable structural phases of 2D Te, also known as tellurene.^[19,20]

Theoretical calculations suggested three different types of phases, namely α , β and γ where, α -phase is the generally stable phase for few-layer tellurene, and β -phase is stable in the monolayer or bilayer form.^[19,21]

Recent experimental works and theoretical calculations have confirmed the existence of mono-layer and few-layered forms of the tellurene, one of the newest members in the 2D semiconductor materials family.^[12,19,22–26] The 2D Te-hexagonal nanoplates were first synthesized on mica substrate by Wang *et al.* *via* van der Waals epitaxy method.^[27] Rather large thickness of these nanoplates (~30–80 nm) beyond atomic scale may reduce their potential for applications in the 2D limit. Later Huang *et al.* successfully fabricated monolayer and few-layer thick tellurene-nanofilms *via* molecular beam epitaxy on graphene.^[23] In contrast to the hexagonal lattice obtained in an earlier work, they obtained rectangular lattices with the in-plane lattice constant of $b = 4.42 \pm 0.05 \text{ \AA}$ and $c = 5.93 \pm 0.05 \text{ \AA}$, which is quite close to lattice parameters of the theoretically predicted monolayer.^[19] Recently, Du *et al.* have synthesized air-stable 2D tellurene by using substrate-free solution process which has high carrier mobility of $\sim 700 \text{ cm}^2/\text{V}\cdot\text{s}$.^[12] They have also fabricated field effect transistor by using a 16 nm thick nanoflake which shows very large on/off ratio of $\sim 10^6$.^[12] One of the main constraints of the previously reported processes is the use of toxic hydrazine hydrate and it requires a relatively high temperature (160–250 °C) for synthesis.^[9,12,22,23,26] Only a few reports describe the synthesis of tellurene in the 2D form utilizing either a substrate-free solution reaction at 180 °C or a probe sonicator with 200–500 W powers.^[7,24,25,28]

Herein, we have synthesized the free-standing few-layer 2D tellurene at room temperature by using simple mechanical stirring technique. Mechanical stirring of bulk Te powders in N-methyl-2-pyrrolidone (NMP) generates few-layer tellurene. The as exfoliated tellurene suspension is stable for up to several weeks under ambient conditions. Transmission electron microscopy (TEM) and atomic force microscopy (AFM) confirm the formation of high crystalline few-layer tellurene nanosheets

[a] A. Bhui, Dr. S. Roychowdhury, Prof. Dr. K. Biswas
New Chemistry Unit
Jawaharlal Nehru Centre for Advanced Scientific Research
(JNCASR)

Jakkur P.O., 560064 Bangalore, India
E-mail: kanishka@jncasr.ac.in

[b] Dr. A. Sen, Prof. Dr. U. V. Waghmare
Theoretical Sciences Unit
Jawaharlal Nehru Centre for Advanced Scientific Research
(JNCASR)

Jakkur P.O., 560064 Bangalore, India

[c] Prof. Dr. K. Biswas
School of Advanced Materials and International Centre of
Materials Science
Jawaharlal Nehru Centre for Advanced Scientific Research
(JNCASR)

Jakkur P.O., 560064 Bangalore, India

Supporting information for this article is available on the WWW under <https://doi.org/10.1002/zaac.202200097>

with large lateral thickness ($\sim 1\text{--}1.6\ \mu\text{m}$). High-resolution TEM (HRTEM) study indicates the formation of both the α - and β -phases of tellurene. Raman spectroscopy suggests the presence of strain in the few-layer tellurene nanosheets. Our first-principles density functional theory (DFT) based phonon dispersion confirms the stability of bilayer β -tellurene in which adjacent layers are held together by weak interlayer van der Waals forces. Electronic structure of bilayer β -tellurene exhibits indirect band gap which decreases with increasing the number of layers.

Bulk tellurium (Te) crystallizes in a trigonal structure (t) (space group $P3_121$) and consists helical chains along crystallographic c -direction.^[15,16] This chain-like structure of Te exhibits strong anisotropy in the structure because it shows strong intrachain covalent bonds between the neighboring atoms (Te–Te bond) and chains themselves are held together by weak van der Waals (vdW) interaction.^[29] First-principles density functional theory (DFT) proposed the structure of two-dimensional tellurium as α -tellurene (Figure 1a) and β -tellurene (Figure 1b) where four-membered (planar) and six-membered (chair-like) rings remain organized in the two-dimensional lattice of tellurene, respectively.^[19] The bond lengths between

tellurium atoms in tellurene indicates the covalent interaction between the neighboring atoms. Interestingly, in tellurene, Te atoms show multivalency (three- and four-fold coordination) behavior which is different from its bulk counterpart (two-fold coordination).^[19]

Here, we have used a simple solution phase synthesis technique like mechanical stirring of the grounded Te polycrystals in N-methyl-2-pyrrolidone (NMP) (see experimental section) in the room temperature. With time, bulk Te exfoliates into 2D tellurene nanosheets which yielded a colorless dispersion, showing the Faraday–Tyndall effect. Non-exfoliated part was separated *via* centrifugation to produce a stable dispersion with a concentration of about 1 mg/mL. The weak interlayer van der Waals forces among the tellurium chains in t-Te can be overwhelmed in a typical stirring process by using an appropriate solvent to obtain a hypervalent few-layer structure of tellurene.^[3,24] The atoms of tellurene are closer together than those of bulk phase, due to the absence of van der Waals interactions.

The powder X-ray diffraction (PXRD) of the exfoliated nanosheets (drop casted and dried in sample holder) recorded using Cu $K\alpha$ ($\lambda = 1.54056\ \text{\AA}$) radiation, could be indexed based on bulk Te with no other impurity phase within the detection limit of PXRD (Figure 1c). Tellurene nanosheets show broad peaks in XRD along with (101) facet orientation in comparison to the bulk-Te. No significant change in PXRD is observed in the case of both fresh and two-week-old 2D tellurene nanosheets (Figure S1, Supporting Information, SI), indicating good stability of tellurene nanosheets in ambient conditions. The synthesized tellurene nanosheets were free from any substrate-induced strain. Thus, there is a possibility of built-in strain during the size reduction. Accordingly, we have characterized the 2D nanosheets *via* Raman spectroscopy. Figure 1d represents the Raman active modes of both bulk Te and few-layer nanosheets. Bulk Te exhibits three vibrational peaks at 90.4, 119.4 and 139.5 cm^{-1} correspond to E^1 (bond bending), A^1 (chain extension mode where every atom vibrates in the basal plane) and E^2 (asymmetric bond-stretching along c axis) modes,^[12,24,25] respectively. The exfoliated nanosheets also show three similar phonon modes with slight blue-shift (104.4, 122.3 and 141.1 cm^{-1}) compared to bulk analogue, while E^1 mode is too broad and weak.^[12] This blue shift can be attributed to the presence of compressive strain in the system.^[25] More careful analysis reveals that shift in A^1 mode is larger than that of E^2 mode due to the distortion of the basal plane, arising from the reconstructions and rearrangements of bonds during the formation of tellurene. Both the PXRD and Raman results confirm that exfoliated tellurene nanosheets retain its hexagonal crystal structure similar to the bulk Te after the exfoliation process.

The thickness of exfoliated nanosheets is measured *via* atomic force microscope (AFM). The thickness of tellurene nanosheets ranges from ~ 1.2 to ~ 2.8 nm with a lateral dimension of ~ 1 to $\sim 1.6\ \mu\text{m}$ (Figure 1e and f). Previous scanning tunneling microscopy showed that monolayer α -tellurene nanoflake has a thickness of ~ 0.6 nm^[25] and bilayer β -tellurene nanoflake has a thickness of ~ 1 nm.^[22] The AFM

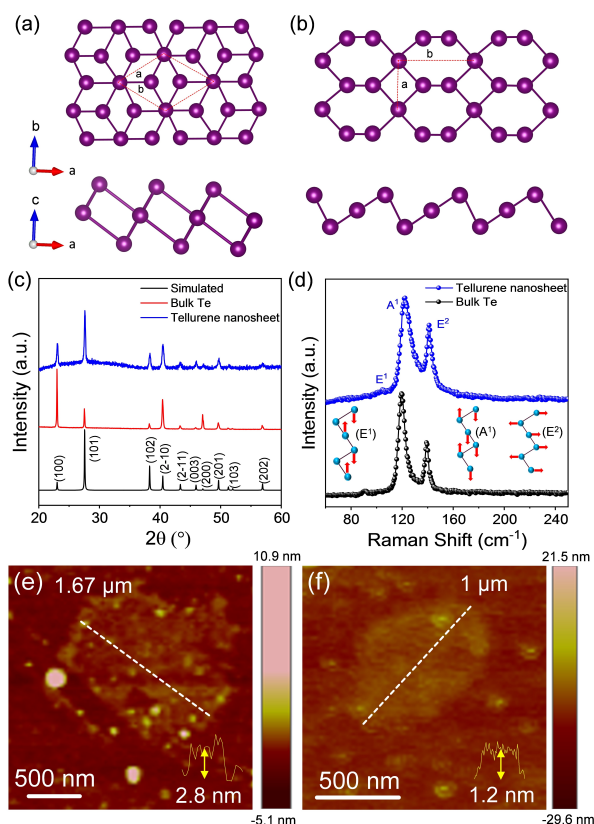


Figure 1. Top (top panel) and side (bottom) views of (a) α and (b) β -tellurene. Unit cells are shown *via* red dashed line. (c) Powder X-ray diffraction pattern and (d) Raman spectra of the nanosheets and bulk-Te powder. AFM images of few-layer tellurene (e and f) representing lateral thickness (white broken line) and the corresponding height profiles (inset).

images therefore corroborate successful synthesis of bilayer and few-layer tellurene nanosheets. Figure 2a–d represents a typical transmission electron microscope (TEM) image of the as synthesized tellurene nanosheet on holey carbon coated Cu grid. High-resolution TEM (HRTEM) images (Figure 2c and d) show the distance between two lattice fringes is 0.323 nm, corresponding to the (101) plane of hexagonal Te.^[24] The single-crystalline feature of the nanosheet is confirmed by selected area electron diffraction (SAED) pattern (Inset of Figure 2c). In addition, the structure of the few-layer tellurene nanosheets is determined in Figure 3a–f by utilizing HRTEM images. Figure 3a and 3b represent atomically resolved HRTEM image of the tellurene nanosheet identifying locations of tellurium atoms. We have joined the atoms through yellow lines in the micrograph Figure 3b and the in-plane lattice constants are measured to be $a \approx 4.4 \text{ \AA}$ and $b \approx 5.6 \text{ \AA}$ (rectangular unit cell), consistent with the previous experimental report^[22] and theoretical prediction of β -tellurene.^[19] Similarly, arrangement of tellurium atoms in Figure 3d and 3f matches with structure of α -tellurene in their top and side views, respectively with a unit cell of $4.4 \times 4.4 \text{ \AA}$ and the distance between two adjacent Te layers (d) is to be $\sim 3.80 \text{ \AA}$ (Figure 3f).^[19,21] The crystal structure and in-plane lattice constants are consistent with the predicted values of α -tellurene phase by Zhu *et al.*^[19] and Dong *et al.*^[30]

We have determined layer-dependent electronic structure and band gap of β -tellurene with and without inclusion of the spin orbit coupling (SOC) in first-principles DFT calculations. As the electronic structure of monolayer β -tellurene is reported earlier,^[19,30,31] we present analysis of the electronic structure of

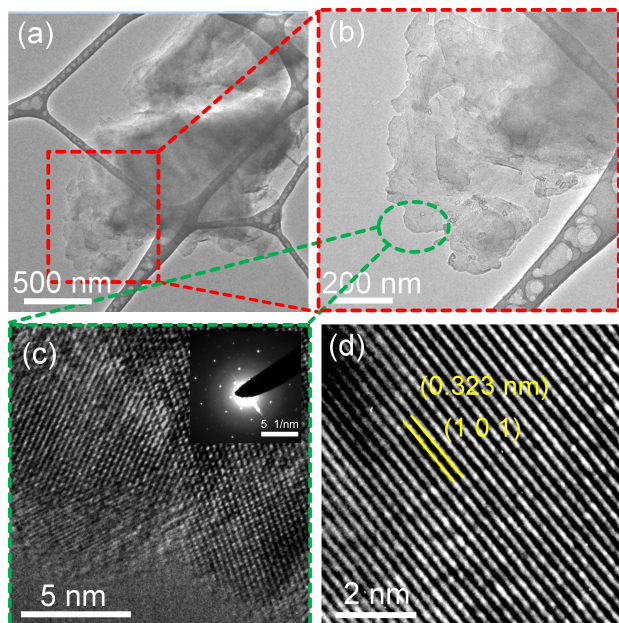


Figure 2. (a) and (b) Typical low-magnification TEM-images of the exfoliated few-layer tellurene nanosheets. (c) and (d) shows high-resolution TEM (HRTEM) images. SAED pattern in the inset of (c) indicates the crystalline nature of the exfoliated tellurene nanosheets. (d) The distance between two lattice fringes is 0.323 nm, corresponding to the (101) plane of hexagonal Te.

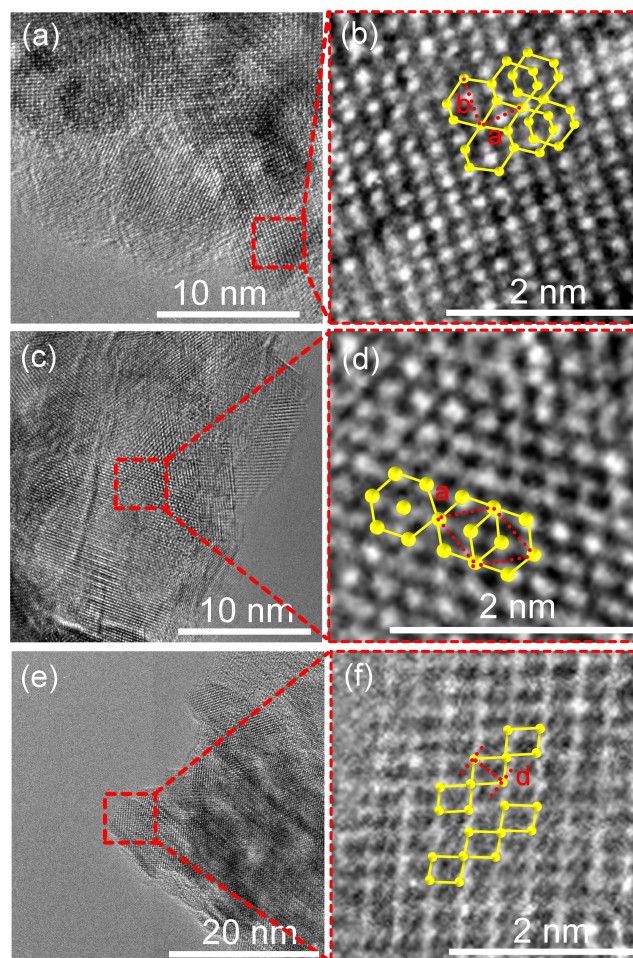


Figure 3. (a) and (b) HRTEM micrographs of drop-casted few-layer tellurene along with schematic models of β -tellurene. Top view of β -tellurene is shown in (b). (c), (d), (e), and (f) HRTEM-micrographs along with schematic models of α -tellurene. Top and side view of α -tellurene are shown in (d) and (f) respectively.

bilayer β -tellurene. As shown in the top view of relaxed bilayer β -tellurene, we used a rectangular unit cell as indicated in Figure S2, SI. Our estimate of the lattice parameter a is 4.26 \AA for the bilayer, which agrees well with the result reported by Wu *et al.*^[31] Our estimate of the lattice parameter b is 5.77 \AA . Lattice parameters obtained from the HRTEM analysis match well with this theoretical data, which supports formation of bilayer β -tellurene. The layer dependent lattice parameters are given in the Table S1, SI. As the number of layers of β -tellurene increase, its lattice parameters increase slightly. Electronic structure of bilayer β -tellurene exhibits an indirect band gap of 1.12 eV and 1.02 eV (Figure 4a and b) for structures optimized without and with vdW-interactions, respectively. With inclusion of the dispersion correction of vdW-interaction using Grimme D2 scheme, the band gap values changed slightly. When the electronic structure was calculated with spin orbit coupling (SOC), the band gap (indirect) of the bilayer is 0.82 eV (Figure 4c). With increasing the number of layers (N), the band

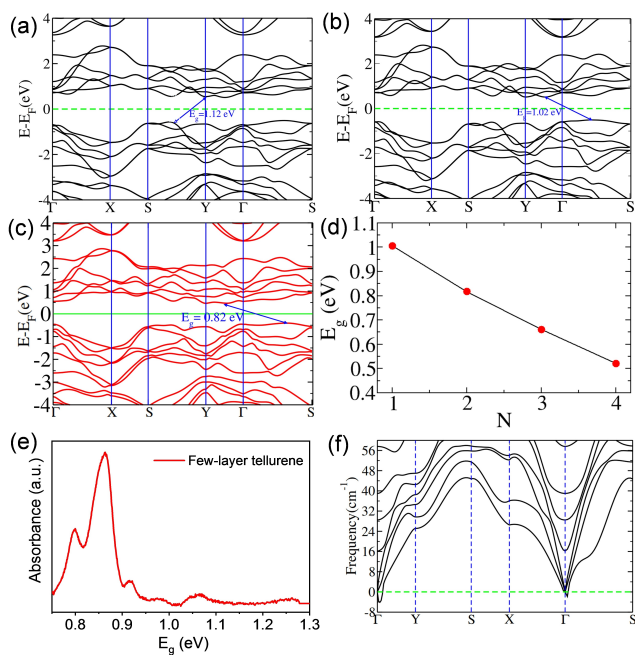


Figure 4. Electronic structure of bilayer tellurene, structure optimised (a) without, and (b) with vdW-interaction. In (c) electronic structure of relaxed bilayer calculated with SOC. (d) Variation in band gap with number of layers (N) of tellurene. (e) Experimental optical absorption spectra of few-layer as synthesized tellurene. (f) Phonon dispersion of bilayer tellurene.

gap using SOC decreases (Figure 4d and Table S2, SI). As implied by our theoretical calculations and previous experimental studies,^[22,23,32] tellurene nanosheets exhibit a thickness dependent band gap varying from mid-infrared to near-infrared region. We have experimentally measured optical absorption spectra to estimate the band gap of the nanosheets in the NMP solution, and interestingly observe several spectral peaks in the near-IR region at 1.25 eV, 1.06 eV, 0.98 eV, 0.90 eV, 0.86 eV, 0.79 eV (Figure 4e). Similar type of spectra have been observed earlier in few-layered phosphorene.^[33] The peaks at ~ 1.25 eV and 1.06 eV are believed to be associated with monolayer and bilayer of tellurene and the other peaks originate from the absorption by thicker nanosheets.

To understand the lattice stability, we calculated phonon dispersion of layered β -tellurene, which shows no unstable modes (Figure S3, SI).^[19] In bilayer tellurene, we find a weakly unstable mode with frequency ~ 4.25 cm^{-1} at Γ point (Figure 4f), which is within the DFT errors associated with broken translational invariance on a mesh. Thereby, bilayer β -tellurene is a stable form, supporting our experimental observation.

In summary, we have successfully synthesized few-layer free-standing nanosheets of tellurene via a simple solution-phase synthesis through mechanical stirring at room temperature. The resulting exfoliated nanosheets are ultrathin (~ 1.2 – 2.8 nm) and exhibit large lateral dimension of ~ 1 – 1.6 μm . Atomically resolved HRETEM images reveal presence of both the stable phases of tellurene viz. α - and β -phases. DFT calculations

confirmed the stability of bilayer β -tellurene, exhibits an indirect band gap of ~ 0.82 eV. With increasing the number of layers, the band gap of tellurene reduces due to quantum confinement effect.

Experimental Section

Reagents. Tellurium (Te, 99.99%, Strategic Metal Investments Ltd.), N-methyl-2-pyrrolidone (NMP, AR 99.5%, SRL chemicals) were used without any further purifications.

Synthesis of few-layer tellurene. Grounded powder of bulk Te of ~ 50 mg was immersed in 10 mL of N-methyl-2-pyrrolidone (NMP) solvent. Then the mixture was sonicated by using a bath sonicator for 5 minutes to make uniform dispersion. The solution was then stirred continuously for 24 hours. After 24 hours of stirring top solution was collected for centrifugation at 2000 rpm for 5 minutes to remove the non-exfoliated part. The precipitated part was then separated from the rest of the solution. Afterward, the rest solution part was centrifuged at 8000 rpm and the precipitated part was collected. The collected flakes were then washed with toluene two times and dried at 50°C in the vacuum oven to further use for characterization.

Powder X-ray diffraction (PXRD). A Bruker D8 diffractometer equipped with $\text{CuK}\alpha$ ($\lambda = 1.5406$ \AA) radiation was used for collecting the PXRD pattern at room temperature. The XRD data were collected of the as-prepared sample and two-weeks air-aged sample after dispersing it in toluene and drop-casting several times in the sample holder.

Raman spectroscopy. Room temperature Raman spectra of the as-synthesized few-layer tellurene were collected by using a LabRAM HR high-resolution Raman spectrometer (Horiba-Jobin Yvon) by using 632 nm wavelength Ar laser.

Optical absorption spectra. A PerkinElmer, Lambda-900 UV/vis/near-IR spectrometer was used to collect the UV-Vis absorption spectra. Optical absorption spectra were recorded after dispersing the sample in NMP.

Atomic force microscopy. A Bruker Innova Microscope was used for carrying out the AFM studies in the tapping mode with a 10 nm diameter containing an antimony-doped silicon tip.

Transmission electron microscopy. A diluted solution of few-layer tellurene dispersed in NMP was used for the TEM studies after drop-casting on a holey carbon-coated Cu grid. An FEI TECNAI G² 20 STWIN TEM operated at 200 kV and an aberration-corrected FEI TITAN3 operated at 300 kV were used for TEM studies.

Computational details. We have performed first-principles calculations based on density functional theory (DFT) which is implemented in the Quantum ESPRESSO package.^[34] Herein, the ionic and core valence electron interactions are modeled with ultrasoft pseudopotentials.^[35] We have used the exchange-correlation energy functional of electrons within a generalized gradient approximation (GGA), parameterized by Perdew, Burke and Ernzerhof.^[36] The energy cutoff was taken as 55Ry to truncate the plane wave basis used in representation of Kohn-Sham wave functions. For representing charge density, we took energy cutoff of 550Ry. We have relaxed the structures for minimization of the energy until the Hellman-Feynman forces on each atom are less than 7.7×10^{-6} eV/ \AA . To simulate a 2D sheet, we have used a periodic supercell including 15 \AA vacuum. In self-consistent Kohn-Sham (KS) calculations of Te with layered form the Brillouin zone (BZ) integrations are sampled over uniform meshes of $20 \times 20 \times 1$. The electronic structure calculations are performed by including

the spin-orbit coupling (SOC) through relativistic pseudopotentials through a second variational procedure.^[37] DFT linear response (implemented in Quantum ESPRESSO^[34] based on Green's function method) was used to determine phonons and dynamical matrices at wave vectors on a $2 \times 2 \times 1$ mesh in the BZ. Using Fourier interpolation dynamical matrices and phonons are found at arbitrary wave vectors in the BZ.

Acknowledgements

K. B. acknowledges support from Science and Engineering Research Board (SERB) (CRG/2019/001306). U. V. W. acknowledges support from J. C. Bose National Fellowship of the SERB-DST. A. B. thanks the CSIR for the fellowship.

Conflict of Interest

The authors declare no conflict of interest.

Data Availability Statement

The data that support the findings of this study are available from the corresponding author upon reasonable request.

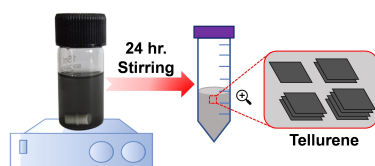
Keywords: Few-layer tellurene · simple synthesis · electronic structure · high resolution transmission electron microscopy · First-principle calculations

- [1] V. Nicolosi, M. Chhowalla, M. G. Kanatzidis, M. S. Strano, J. N. Coleman, *Science* **2013**, *340*, 1226419.
- [2] S. Z. Butler, S. M. Hollen, L. Cao, Y. Cui, J. A. Gupta, H. R. Gutiérrez, T. F. Heinz, S. S. Hong, J. Huang, A. F. Ismach, E. Johnston-Halperin, M. Kuno, V. V. Plashnitsa, R. D. Robinson, R. S. Ruoff, S. Salahuddin, J. Shan, L. Shi, M. G. Spencer, M. Terrones, W. Windl, J. E. Goldberger, *ACS Nano* **2013**, *7*, 2898–2926.
- [3] F. R. Fan, R. Wang, H. Zhang, W. Wu, *Chem. Soc. Rev.* **2021**, *50*, 10983–11031.
- [4] S. Deckoff-Jones, Y. Wang, H. Lin, W. Wu, J. Hu, *ACS Photonics* **2019**, *6*, 1632–1638.
- [5] E. Liu, A. Negm, M. M. R. Howlader, *Mater. Today Energy* **2021**, *20*, 100625.
- [6] A. Apte, S. Kouser, F. Safi Samghabadi, L. Chang, L. M. Sassi, D. Litvinov, B. I. Yakobson, A. B. Puthirath, P. M. Ajayan, *Mater. Today Energy* **2021**, *44*, 40–47.
- [7] B. Qiu, C. Wang, J. Wang, Z. Lin, N. Zhang, L. Cai, X. Tao, Y. Chai, *Mater. Today* **2021**, *21*, 100720.
- [8] Z. Gao, G. Liu, J. Ren, *ACS Appl. Mater. Interfaces* **2018**, *10*, 40702–40709.
- [9] D. Wang, A. Yang, T. Lan, C. Fan, J. Pan, Z. Liu, J. Chu, H. Yuan, X. Wang, M. Rong, *J. Mater. Chem. A* **2019**, *7*, 26326–26333.
- [10] D. Wines, J. A. Kropp, G. Chaney, F. Ersan, C. Ataca, *Phys. Chem. Chem. Phys.* **2020**, *22*, 6727–6737.
- [11] D. K. Sang, B. Wen, S. Gao, Y. Zeng, F. Meng, Z. Guo, H. Zhang, *Nanomaterials* **2019**, *9*, 1075.
- [12] Y. Wang, G. Qiu, R. Wang, S. Huang, Q. Wang, Y. Liu, Y. Du, W. A. Goddard, M. J. Kim, X. Xu, *Nat. Electron.* **2018**, *1*, 228–236.
- [13] W. Wu, G. Qiu, Y. Wang, R. Wang, P. Ye, *Chem. Soc. Rev.* **2018**, *47*, 7203–7212.
- [14] Z. Shi, R. Cao, K. Khan, A. K. Tareen, X. Liu, W. Liang, Y. Zhang, C. Ma, Z. Guo, X. Luo, *Nano-Micro Lett.* **2020**, *12*, 99.
- [15] A. von Hippel, *J. Chem. Phys.* **1948**, *16*, 372–380.
- [16] C. Adenis, V. Langer, O. Lindqvist, *Acta Crystallogr. Sect. C* **1989**, *45*, 941–942.
- [17] B. Mayers, Y. Xia, *J. Mater. Chem. C* **2002**, *12*, 1875–1881.
- [18] M. Mo, J. Zeng, X. Liu, W. Yu, S. Zhang, Y. Qian, *Adv. Mater.* **2002**, *14*, 1658–1662.
- [19] Z. Zhu, X. Cai, S. Yi, J. Chen, Y. Dai, C. Niu, Z. Guo, M. Xie, F. Liu, J.-H. Cho, Y. Jia, Z. Zhang, *Phys. Rev. Lett.* **2017**, *119*, 106101.
- [20] L. Xian, A. Pérez Paz, E. Bianco, P. M. Ajayan, A. Rubio, *2D Mater.* **2017**, *4*, 041003.
- [21] J. Qiao, Y. Pan, F. Yang, C. Wang, Y. Chai, W. Ji, *Sci. Bull.* **2018**, *63*, 159–168.
- [22] J. Chen, Y. Dai, Y. Ma, X. Dai, W. Ho, M. Xie, *Nanoscale* **2017**, *9*, 15945–15948.
- [23] X. Huang, J. Guan, Z. Lin, B. Liu, S. Xing, W. Wang, J. Guo, *Nano Lett.* **2017**, *17*, 4619–4623.
- [24] Z. Xie, C. Xing, W. Huang, T. Fan, Z. Li, J. Zhao, Y. Xiang, Z. Guo, J. Li, Z. Yang, B. Dong, J. Qu, D. Fan, H. Zhang, *Adv. Funct. Mater.* **2018**, *28*, 1705833.
- [25] S. Khatun, A. Banerjee, A. J. Pal, *Nanoscale* **2019**, *11*, 3591–3598.
- [26] M. Amani, C. Tan, G. Zhang, C. Zhao, J. Bullock, X. Song, H. Kim, V. R. Shrestha, Y. Gao, K. B. Crozier, *ACS Nano* **2018**, *12*, 7253–7263.
- [27] Q. Wang, M. Safdar, K. Xu, M. Mirza, Z. Wang, J. He, *ACS Nano* **2014**, *8*, 7497–7505.
- [28] H. Cui, K. Zheng, Z. Xie, J. Yu, X. Zhu, H. Ren, Z. Wang, F. Zhang, X. Li, L.-Q. Tao, H. Zhang, X. Chen, *ACS Appl. Mater. Interfaces* **2020**, *12*, 47704–47713.
- [29] P. Ghosh, J. Bhattacharjee, U. V. Waghmare, *J. Phys. Chem. C* **2008**, *112*, 983–989.
- [30] Y. Dong, B. Zeng, X. Zhang, D. Li, J. He, M. Long, *J. Appl. Phys.* **2019**, *125*, 064304.
- [31] B. Wu, X. Liu, J. Yin, H. Lee, *Mater. Res. Express* **2017**, *4*, 095902.
- [32] J. Peng, Y. Pan, Z. Yu, J. Wu, J. Wu, Y. Zhou, Y. Guo, X. Wu, C. Wu, Y. Xie, *Angew. Chem. Int. Ed.* **2018**, *57*, 13533–13537; *Angew. Chem.* **2018**, *130*, 13721–13725.
- [33] P. Yasaei, B. Kumar, T. Foroozan, C. Wang, M. Asadi, D. Tuschel, J. E. Indacochea, R. F. Klie, A. Salehi-Khojin, *Adv. Mater.* **2015**, *27*, 1887–1892.
- [34] P. Giannozzi, S. Baroni, N. Bonini, M. Calandra, R. Car, C. Cavazzoni, D. Ceresoli, G. L. Chiarotti, M. Cococcioni, I. Dabo, A. Dal Corso, S. de Gironcoli, S. Fabris, G. Fratesi, R. Gebauer, U. Gerstmann, C. Gougoussis, A. Kokalj, M. Lazzeri, L. Martin-Samos, N. Marzari, F. Mauri, R. Mazzarello, S. Paolini, A. Pasquarello, L. Paulatto, C. Sbraccia, S. Scandolo, G. Sclauzero, A. P. Seitsonen, A. Smogunov, P. Umari, R. M. Wentzcovitch, *J. Phys. Condens. Matter* **2009**, *21*, 395502.
- [35] D. Vanderbilt, *Phys. Rev. B* **1990**, *41*, 7892–7895.
- [36] J. P. Perdew, K. Burke, M. Ernzerhof, *Phys. Rev. Lett.* **1996**, *77*, 3865–3868.
- [37] A. D. Corso, A. M. Conte, *Phys. Rev. B* **2005**, *71*, 115106.

Manuscript received: March 3, 2022

Revised manuscript received: May 12, 2022

Accepted manuscript online: May 15, 2022



*A. Bhui, Dr. S. Roychowdhury, Dr. A. Sen, Prof. Dr. U. V. Waghmare, Prof. Dr. K. Biswas**

1 – 6

Free-Standing Few-Layer Tellurene Nanosheets: Simple Solution-Phase Synthesis and Electronic Structure

